



PCCP

QM/MM MD Simulations Reveal an Asynchronous PCET mechanism for the Nitrite Reduction by Copper Nitrite Reductase

Journal:	<i>Physical Chemistry Chemical Physics</i>
Manuscript ID	CP-ART-06-2020-003053.R1
Article Type:	Paper
Date Submitted by the Author:	13-Aug-2020
Complete List of Authors:	Cheng, Ronny; Xiamen University, State Key Laboratory of Physical Chemistry of Solid Surfaces and Fujian Provincial Key Laboratory of Theoretical and Computational Chemistry Cao, Zexing; Xiamen University, Department of Chemistry Wu, Chun; Rowan University, Cao, Zexing; Xiamen University, Department of Chemistry Wang, binju; College of Chemistry and Chemical Engineering, Xiamen University, Xiamen, China, department of chemistry; Xiamen University,

SCHOLARONE™
Manuscripts

ARTICLE

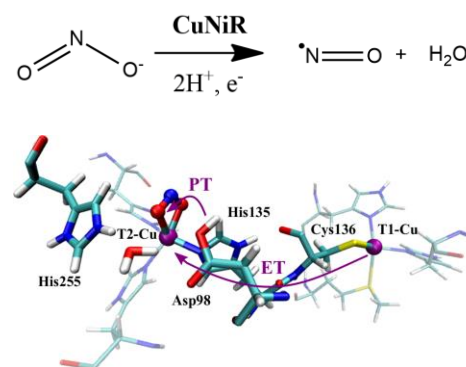
QM/MM MD Simulations Reveal an Asynchronous PCET mechanism for the Nitrite Reduction by Copper Nitrite Reductase

Ronny Cheng,^a Chun Wu,^{b*} Zexing Cao^{a*} and Binju Wang^{a*}

Received 00th January 20xx,
Accepted 00th January 20xx

DOI: 10.1039/x0xx00000x

Nitrite reductases are enzymes that aid in the denitrification process by catalyzing the reduction of nitrite to nitric oxide gas. Since this reaction is the first committed step that involves gas formation, it is regarded to be a vital step for denitrification. However, the mechanism of copper-containing nitrite reductase is still under debate due to discrepancy between theoretical and experimental data, especially in terms of the roles of secondary shell residues Asp98 and His255 and the electron transfer mechanism between two copper sites. Herein, we revisited the nitrite reduction mechanism of *A. faecalis* copper nitrite reductase using QM(B3LYP)/MM-based metadynamics. It is found that the intramolecular electron transfer from T1-Cu to T2-Cu occurs via an asynchronous proton-coupled electron transfer (PCET) mechanism, with electron transfer (ET) preceding proton transfer (PT). In particular, we found that the ET process is driven by the conformation conversion of Asp98 from gatekeeper to proximal one, which is much more energy-demanding than the PCET itself. These results highlight that the inclusion of electron donor is vital to investigate the electron-transfer related processes like PCET.



Introduction

Rapid industrialization has led to an imbalance in the global nitrogen cycle, as the rate of nitrogen fixation has far exceeded the rate of denitrification due to its role in fertilizer production.¹⁻⁴ Thus, strategies in rebalancing the global nitrogen cycle is being done to avoid negative environmental effects such as eutrophication of marine ecosystems, increased acidity of ecosystems and production of greenhouse gas nitric oxide. Denitrification is an important environmental process as it facilitates the decomposition of nitrogen-containing compounds to nitrogen gas.⁴ This is facilitated by various

denitrifying enzymes found in denitrifying bacteria, including nitrite reductase which catalyzes the reduction of nitrite to nitric oxide. Since nitrite reduction is the first committed step to produce gaseous product, it is considered as the critical step in the denitrification process.⁴ Nitrite reductases can be classified into two types according to its metal cofactors: (1) cd1-heme containing nitrite reductase and (2) copper containing nitrite reductases (CuNiR).⁵

CuNiRs present in thermophilic and non-thermophilic denitrifying bacteria are structurally homologous across species, characterized as a homotrimeric enzyme with each ~37 kDa monomer containing one T1 copper site and one T2 copper site (see Figure 1).⁵ The T1 copper site is characterized in

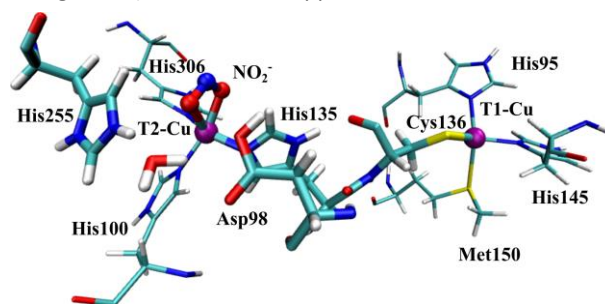


Figure 1. Schematic diagram of relevant residues of nitrite-bound *A. faecalis* CuNiR.⁵ This includes residues ligated to both T1-Cu and T2-Cu sites, and secondary shell residues Asp98 and His255.

^a State Key Laboratory of Physical Chemistry of Solid Surfaces and Fujian Provincial Key Laboratory of Theoretical and Computational Chemistry, College of Chemistry and Chemical Engineering, Xiamen University, Xiamen 361005, P. R. China

^b College of Science and Mathematics, Rowan University, Glassboro, NJ, 08028 USA

Correspondence: Binju Wang, wangbinju2018@xmu.edu.cn

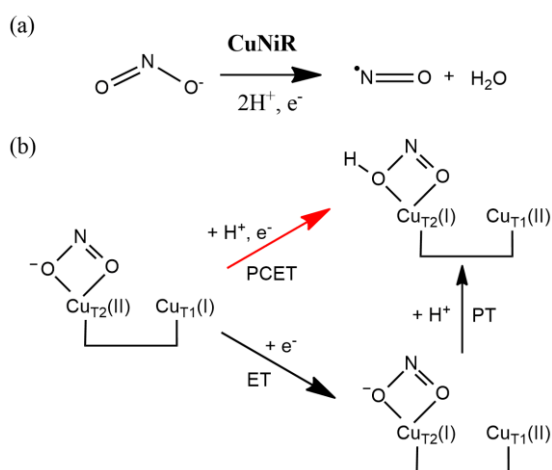
Zexing Cao, zxcao@xmu.edu.cn

Chun Wu, wuc@rowan.edu

Electronic Supplementary Information (ESI) available: [details of any supplementary information available should be included here]. See

DOI: 10.1039/x0xx00000x

crystallography by having a His₂-Cys-Met ligation with tetrahedral geometry, which acts as the electron reservoir site of the enzyme. The reserved electron at T1-Cu can be subsequently donated to T2-Cu upon nitrite reduction.⁵⁻¹¹ The T2 copper site serves as the catalytic center of the enzyme and is ligated with three histidine residues and its substrate NO₂⁻. Both copper sites are spaced around 12.6 Å apart and are connected via two protein links, a bridge connecting His135 and Cys136, and a sensor loop that contains residues between His95 to Asp98.⁵⁻¹¹



Scheme 1. (a) Reaction catalyzed by CuNiR; (b) Proposed mechanisms for intramolecular electron transfer from T1-Cu to T2-Cu.^{9, 12-16}

The reduction mechanism of copper nitrite reductase (CuNiR) is still under debate due to conflicting evidence between crystallographic, spectroscopic and computational data.^{8, 9, 11, 16-21} Studies agree that nitrite binding, intramolecular electron transfer (ET) from T1-Cu to T2-Cu, proton transfer (PT) to nitrite, and product release are all involved in nitrite reduction. However, questions surrounding the protonation states of secondary shell residues Asp98 and His255 and the mechanism on how intramolecular ET occurs remain unresolved. Kinetic studies and DFT studies suggest that nitrite binding undergoes a random sequential mechanism, wherein nitrite binding does not depend on the oxidation state of T2-Cu as it can occur before or after intramolecular ET.^{12, 15, 18, 20} However, an ordered mechanism was also suggested, with nitrite binding occurring before intramolecular ET, citing the low binding affinity of NO₂⁻ in the reduced T1-Cu(I) state.²¹⁻²³ Moreover, it was found that the reduction potentials in T1-Cu and T2-Cu were nearly equal, suggesting that intramolecular ET prior to nitrite binding is thermodynamically unfavorable.²⁴ While intramolecular ET and PT are required processes in nitrite reduction, occurrence of proton-coupled electron transfer (PCET) was also suggested on the basis of solvent kinetic isotope effect studies (see Scheme 1b).¹² However, the nature of PCET, e.g. whether the thermodynamically unfavorable PT step is preceding ET or if both PT and ET are concerted, is still unknown.¹² The former case was suggested in recent experimental studies,^{13, 14} while most of previous

computational studies treat intramolecular ET and PT as separate processes.¹⁶⁻¹⁹

Existing studies have already established the importance of Asp98 and His255 in the reduction mechanism of CuNiR based on the pH of optimal activity, which is between 5 to 7, which is closely correlated to the pH dependence of intramolecular ET in nitrite-bound CuNiR.^{24, 25} Mutagenesis studies also show that mutations of these two residues result in substantially decreased enzymatic activity.²⁵ Furthermore, mutagenesis of His135 and Cys136 show loss of enzymatic activity, indicating its vital role in nitrite reduction.²⁶⁻²⁸ Neutron crystallography has been used to solve the protonation state issue, but the assigned protonation states of the resting state in the absence of substrate NO₂⁻ may not be relevant to catalysis.^{10, 11}

This study focuses on investigating the nitrite reduction mechanism, especially of the intramolecular electron transfer from T1-Cu to T2-Cu of *A. faecalis* CuNiR using QM(B3LYP)/MM-based metadynamics.²⁹⁻³¹ Upon the inclusion of electron donor T1-Cu domain, we demonstrate that the reaction successfully leads to a PCET process, in which the proton transfer from Asp98 is coupled with the electron transfer from T1-Cu(I) to T2-Cu(II). In particular, we found that the ET process is driven by the conformation conversion of Asp98 from gatekeeper to proximal one. This enhances our fundamental understanding of CuNiR, which can be helpful for developing amperometric biosensors or for biomedical applications.³²

Methods

System Preparation

The starting point of the model is the crystal structure of *A. faecalis* CuNiR bound to nitrite which was obtained from RCSB (PDB ID: 1SJM).⁶ Two monomer units were included in the model, including one T1-Cu site and one T2-Cu site. Force field parameters attributed to the metal site environment of both copper sites were added using the Metal Center Parameter Builder (MCPB.py) under AmberTools18.³³⁻³⁶ Modeling was done such that the oxidation states of T1-Cu and T2-Cu were set at the reduced T1-Cu(I) state and the oxidized T2-Cu(II) state, respectively. The Amber ff14SB force field was employed to treat the protein residues.³⁷ Necessary input files for MD simulations were produced through tleap, with the system solvated using TIP3P water by filling a rectangular box encompassing up to 15 Å from the protein surface.^{37, 38} Adequate Na⁺ and Cl⁻ ions were added to maintain electroneutrality of the system.

MD Simulations

Molecular dynamics simulations for three possible protonation configurations were done using CUDA-accelerated sander under AMBER18.^{33, 39-42} These protonation configurations include the following: (1) deprotonated Asp98 and protonated His255 (ASP-HIP), (2) protonated Asp98 and deprotonated His255 (ASH-HID) and (3) protonated Asp98 and protonated His255 (ASH-HIP). Energy minimization was first performed using steepest descent and conjugate gradient

method. This was followed by gently annealing the system from 10 to 300 K in the canonical ensemble. The system was then equilibrated without any restraints in the NPT ensemble for 2 ns at the target temperature of 300 K and the target pressure of 1.0 atm using the Langevin thermostat⁴³ and Berendsen barostat,⁴⁴ with collision frequency of 2 ps and pressure relaxation time of 1 ps. After that, a productive MD run was performed for 100 ns. During all MD simulations, long-range interactions were considered through the Particle Mesh Ewald method,⁴⁵ with bond lengths involving hydrogen atoms constrained through SHAKE⁴⁶ with an integration step of 2 fs.

QM/MM Metadynamics Simulations

A representative snapshot for each protonation state was obtained from the MD simulation as initial input to perform QM(B3LYP)/MM-MetD using cp2k,⁴⁷ where the QM and MM components are handled by QUICKSTEPS⁴⁸ and FIST,⁴⁷ respectively. The QM region is treated with DFT (B3LYP) using a dual basis set of Gaussian and plane-waves (GPW) formalism, while the MM region is treated similarly as with classical MD simulations. The B3LYP hybrid functional is utilized as it is widely used and is demonstrated to be successful for studying metalloenzymes.^{49–52} DFT calculations were performed using the Gaussian double- ζ valence polarized (DZVP) basis set, while an auxiliary plane-wave basis set with a cutoff of 360 Ry was used to converge the electron density, in conjunction with Geodecker-Teter-Hutter (GTH) pseudopotentials^{48,53} for treating the core electrons. The auxiliary density matrix method (ADMM) was used to speed up Hartree-Fock exchange calculations, with the Cu atom treated using the FIT12 auxiliary basis set, and the rest treated with the cpFIT3 auxiliary basis set.⁵⁴ Hydrogen link atoms were added in bonds crossing the QM/MM boundary to separate both regions.

The QM region includes the T1-Cu and T2-Cu sites alongside the sidechains of Asp98, His255, His135 and Cys136. As we were also interested in the effects of T1-Cu site on reduction, a separate QM region was set-up without the T1-Cu site. The charge and multiplicity of the QM region were then set accordingly. Geometry optimization was first performed, followed by QM/MM MD equilibration without any restraint for 1 ps. Well-tempered metadynamics simulations were then performed to explore the free energy landscape for PCET and product release.^{29–31} All calculations were performed under the NVT ensemble using an integration step of 0.5 fs. Simulations were run until the transition state was crossed, as recommended for simulations of chemical reactions.³¹ The Gaussian height was set to 0.6 kcal/mol while the deposition rate of Gaussian hills was set to 10 fs.

Results

Initial State of *A. faecalis* CuNiR

The starting point in these simulations is the nitrite-bound state of *A. faecalis* CuNiR. Classical MD simulations of the system show good superposition with the crystal structure (Figure S1). As we are interested in the conditions necessary for

nitrite reduction, the system was prepared based on the oxidized T2-Cu(II)-NO₂⁻ and reduced T1-Cu(I) state, in accordance with existing EXAFS and X-ray crystallography studies.^{21–23}

Since the protonation states of Asp98 and His255 are key to the mechanism of CuNiR, different protonation states of Asp98 and His255 were considered in our study. The possibility of both Asp98 and His255 being deprotonated was already ruled out, since experiments show that the nitrite reduction did not occur at basic conditions.^{24, 25} The case where Asp98 is deprotonated and His255 is protonated was also ruled out, as our QM/MM-MD equilibration shows it converged to the protonation state where Asp98 is protonated and His255 is deprotonated (Figure S2). Thus, our study will focus on two possible protonation states, in the first both Asp98 and His255 are protonated (ASH-HIP), and in the second Asp98 is protonated while His255 is deprotonated (ASH-HID).

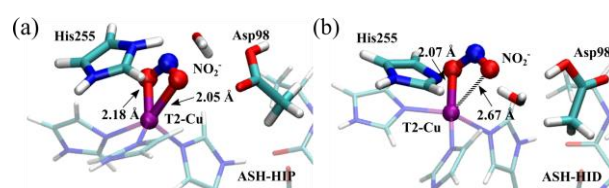


Figure 2. (a) The T2-Cu(II)-NO₂⁻ binding mode at equilibrium of the ASH-HIP protonation state. (b) The T2-Cu(II)-NO₂⁻ binding mode at equilibrium of the ASH-HID protonation state. Equilibrium average distances between T2-Cu and both oxygen atoms of nitrite are given accordingly.

Inspection of the equilibrium structures of the nitrite-bound state in ASH-HIP and ASH-HID protonation states show different binding modes of nitrite, as illustrated in Figure 2. In the case of ASH-HIP, QM(B3LYP)/MM-MD simulations show a bidentate η -O,O binding mode for NO₂⁻, with the average distances from T2-Cu to both oxygen atoms being 2.05 Å and 2.18 Å, respectively. In contrast, in the ASH-HID state NO₂⁻ shows a monodentate η -O binding form, with the shorter Cu-O distance of 2.07 Å and the longer Cu-O distance of 2.67 Å. Comparison of the equilibrium geometry of T2 copper site show that the binding mode of NO₂⁻ in the ASH-HIP protonation state is more consistent with existing crystal structures. The nitrite reduction occurring in the ASH-HIP protonation state will be further investigated.

Nitrite Reduction is Initiated by Proton-coupled Electron Transfer

To unravel the role of the T1 copper site in the nitrite reduction mechanism, QM(B3LYP)/MM-MetD simulations were performed for PCET process with and without considering the T1 copper site as part of the QM region. Figure 3 shows the calculated free energy profile of the PCET process for the QM region without T1 copper site, which shows that the proton transfer from Asp98 to nitrite is highly unfavorable kinetically and thermodynamically.

In light of above findings, the electron donor T1-Cu(I) was incorporated into QM region. First, the plausible electron transfer pathway was identified using the Pathways plugin of VMD.⁵¹ The pathway plug-in, which takes into account the coupling based on covalent bonds, H-bonds and through-space

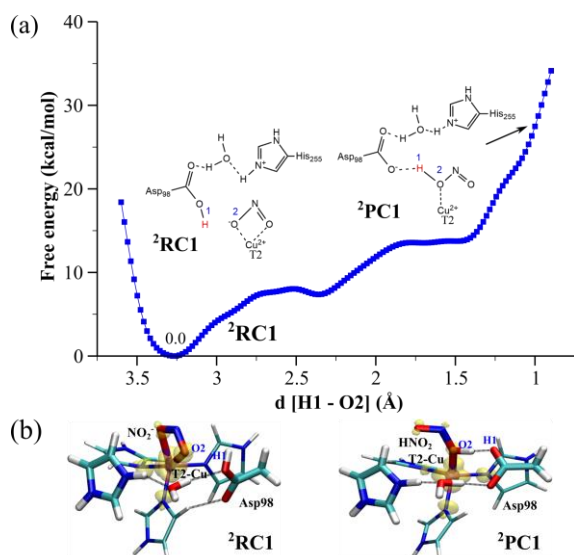


Figure 3. (a) The QM(B3LYP)/MM-MetD calculated free-energy profile for proton transfer from Asp98 to NO_2^- moiety in T2-Cu(II) oxidized state of CuNiR. The reaction coordinate is defined as the distance difference between O2 of nitrite and H1 of Asp98. (b) The representative structures of the QM region along the reaction pathway, with spin-up isodensity surfaces plotted in yellow.

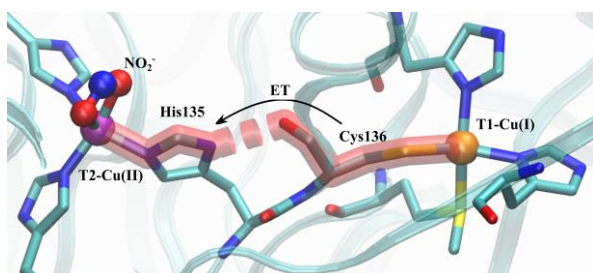


Figure 4. Representation of the electron transfer pathway via the H-bond bridge between His135 and Cys136, which was analyzed through the Pathways plugin of VMD.⁵⁵ His135 and Cys136 are ligated to the T2-Cu and T1-Cu, respectively.

jumps between electron donor and electron acceptor, enables us to identify and visualize electron tunnelling pathways, as well as calculations of relative electronic couplings.⁵⁵ A visualization of the ET pathway is shown in Figure 4, and it can be seen that the electron could pass through an H-bonding network formed by His135 and Cys136. This ET pathway provides evidence that His135 and Cys136 are the key residues involved in the intramolecular electron transfer from T1-Cu to T2-Cu, which can explain the loss of enzymatic activity observed in mutagenesis of His135 and Cys136.²⁶⁻²⁸

As such, the electron transfer bridging residues His135, Cys136 and the electron donor T1-Cu domain were incorporated into the QM region to investigate the subsequent PCET process. Figure 5 shows the QM(B3LYP)/MM-MetD calculated free energy profile. It is seen that the proton transfer from Asp98 is coupled with the electron transfer from T1-Cu(I) to T2-Cu(II), involving an Gibbs energy barrier of ~ 17.0 kcal/mol. These results highlight the importance of the T1-Cu site in the

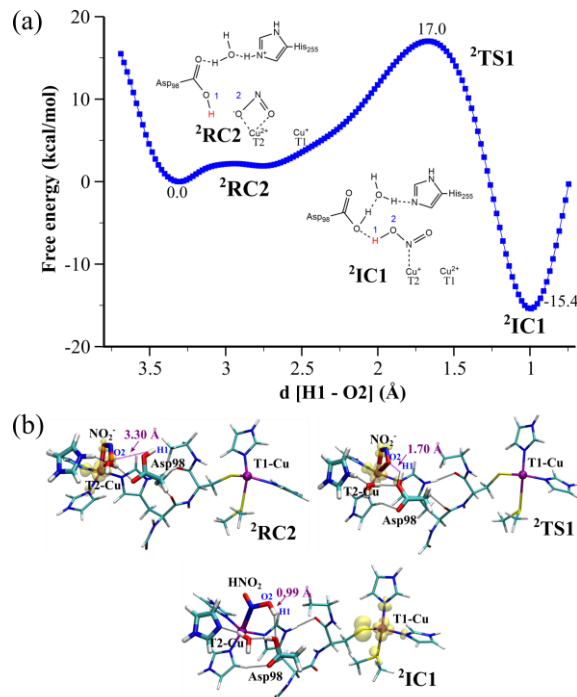


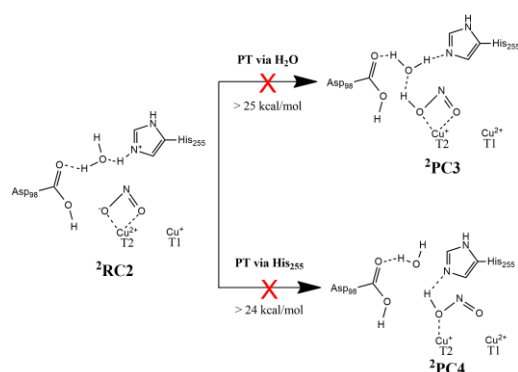
Figure 5. (a) The QM(B3LYP)/MM-MetD calculated free-energy profile for proton transfer from Asp98 in CuNiR. The reaction coordinate is defined as the distance difference between O2 of nitrite and H1 of Asp98. The width of the Gaussian shaped potential hills was set to 0.25 Å. (b) The representative structures of the QM region along the reaction pathway, with spin-up isodensity surfaces plotted in yellow. The distance between the O2 of nitrite and the H1 of Asp98 is marked accordingly.

mechanism of nitrite reduction. Upon the inclusion of electron donor T1-Cu domain, the reaction leads successfully to a PCET process, wherein the electron passes through the H-bonding networks formed by His135 and Cys136 bridge.

To verify the PCET mechanism demonstrated in Figure 5, QM(B3LYP)/MM-MetD calculations were also performed with the relatively larger triple- ζ valence polarized (TZVP) Gaussian basis set. As shown in Figure S3, the QM/MM metadynamics with TZVP basis set yields a Gibbs energy barrier of 17.2 kcal/mol for the PCET process, which is quite similar to 17.0 kcal/mol obtained with the DZVP basis set, while the both values are consistent with the experimental value of 16.8 kcal/mol derived from the rate constant²⁵ according to transition state theory. Thus, use of DZVP basis set is adequate to compute the free energy profiles for the present system.

Proton Transfer Occurs from Asp98 to Nitrite

In the last section, we show that nitrite reduction is initiated by proton-coupled electron transfer (Figure 5), wherein both Asp98 and His255 are protonated. In addition to the above proton transfer route, we also investigated the possible proton transfer routes either directly from His255 or via bridging water. As summarized in Scheme 2, the proton transfer either directly from His255 or via bridging water are found to be kinetically unfavorable in terms of high free energy barriers (Figures S4 and



Scheme 1. QM(B3LYP)/MM-MetD calculated free energy barriers of PCET process, in which the proton transfers either directly from His255 to nitrite (bottom) or via the bridging water to nitrite (top) are both found to be kinetically unfavorable.

S5). These results highlight the significance of Asp98 as the proton source for nitrite reduction, which is line with previous DFT model calculations.^{16, 18}

For comparison, we also investigated the PCET process in the ASH-HID protonation state, in which Asp98 is protonated while His255 is in the neutral form. However, the corresponding PCET process is calculated to be highly unfavorable (Figure S6). Taken together, our calculations support that ASH-HIP protonation state is required to mediate a PCET process toward nitrite reduction, which involves a free energy barrier of 17.0 kcal/mol.

The nature of electron transfer from the T1-Cu site to the T2-Cu site

With both copper sites and the electron transfer bridge considered in the QM region, the reduction reaction is effectively an asynchronous PCET as depicted in Figure 5. This is in contrast to the experimental proposal that ET and PT occurs as separate elementary steps.^{12, 14}

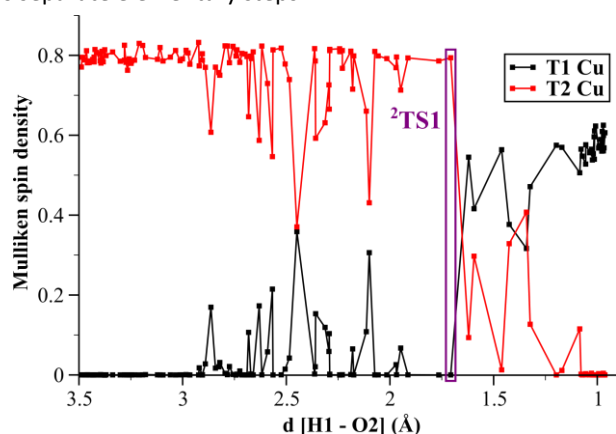


Figure 6. The calculated spin density on both coppers along the QM(B3LYP)/MM-MetD simulations of the PCET step in Figure 5.

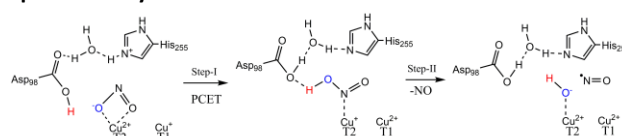
QM(B3LYP)/MM-MetD provide interesting details about the PCET mechanism of CuNiR. Figure 6 shows the mulliken charge evolution of both coppers along QM(B3LYP)/MM-MetD simulations. It is seen that the spin density of both copper sites is maintained between the reactant state (${}^2\text{RC}2$) and the

transition state (${}^2\text{TS}1$), indicating that ET has not yet occurred. ET occurs only if the distance between protonated Asp98 and O2 atom of nitrite is below ~ 1.7 Å, which coincides to the transition state in Figure 5. What can be observed in ${}^2\text{TS}1$, however, is a switch in Asp98 conformation from the gatekeeper to the proximal conformation, which occurs as the nitrite O2—Asp98 H1 distance moves closer from ~ 3.30 Å in ${}^2\text{RC}1$ state to ~ 1.70 Å in ${}^2\text{TS}1$, as illustrated in Figure 5b. Thus, our simulations confirm that nitrite binding occurs before intramolecular ET. First, we did not observe spontaneous ET from T1-Cu to T2-Cu throughout QM/MM MD simulations. Second, using QM/MM metadynamics, we found the ET occurs only when the distance between the protonated ASP98 and O2 atom of nitrite is decreased to ~ 1.70 Å. In such proximal conformation of Asp98, the reduction potential of T2-Cu active site can be elevated, which drives the long-range ET from T1-Cu to T2-Cu.

Once the proton of Asp98 moves closer to nitrite in the proximal conformation, the reduction potential of T2-Cu active site can be elevated, which drives the long-range ET from T1-Cu to T2-Cu. As the electron transfer occurs at the O2—H1 distance of ~ 1.7 Å, this indicates that ET preceded PT. As judged from the calculated free energy profile in Figure 5, the gatekeeper to proximal conformation conversion is much more energy-demanding than the PCET itself, while the latter process is quite facile starting from the proximal conformation of Asp98. Inspection of the geometry of ${}^2\text{IC}1$ indicates that nitrite has been reduced into HNO_2 . The binding mode of the substrate switches to the monodentate $\eta\text{-N}$ mode. The oxidation states of both copper sites are flipped in this state, indicating the completion of intramolecular electron transfer. Asp98 remains to be in protonated form while His255 is in neutral state.

Overall, it is observed that intramolecular electron transfer from T1-Cu to T2-Cu occurs via an asynchronous PCET mechanism, which is facilitated by conformation change of Asp98 from gatekeeper to proximal conformation. Calculations using different population analysis methods and basis set do not affect the trend of the ET process (Figure S7).

Proposed Catalytic Mechanism of CuNiR



Scheme 2. Proposed reduction mechanism of *A. faecalis* CuNiR based on QM(B3LYP)/MM-MetD simulations.

Based on QM(B3LYP)/MM-MetD simulations, a new catalytic mechanism of CuNiR is proposed as shown in Scheme 3. In line with previous DFT calculations,^{16, 18} the catalysis requires that both Asp98 and His255 are in their protonated states. Previous DFT studies suggest that the nitrite reduction is achieved by the stepwise PT and ET, with ET occurring prior to PT.^{16, 18} However, for the first time, our study demonstrates that nitrite reduction is initiated by an asynchronous PCET mechanism, in which the proton transfer from Asp98 to nitrite

is driven by the long-range electron transfer from T1-Cu(I) to T2-Cu(II).

We dissect the components of the PCET of CuNiR, which includes the intramolecular ET via the H-bonding network between His135 and Cys136 and the proton transfer from Asp98 to nitrite. Prior to PCET, a conformational change of Asp98 from gatekeeper to proximal is required, which is more energy demanding compared to PCET itself. The calculated Gibbs energy barrier for overall PCET is 17.0 kcal/mol, which is in agreement with experimental and DFT studies.^{16, 18, 25} The experimental free energy barrier of 16.8 kcal/mol is derived from the rate constant according to transition state theory.²⁵

After PCET, product release occurs via a favorable HO---NO bond cleavage (Step-II in Scheme 3), with a Gibbs energy barrier of 12.1 kcal/mol (Figure S8). The reaction leads to the formation of T2-Cu(II)-OH⁻ species and NO product. Throughout the N—O cleavage process, the reduced T1-Cu(I) state is maintained, indicating it is not involved in N-O cleavage reaction. The calculated product release mechanism herein is in agreement with recent DFT studies,^{17, 18} suggesting the formation of the T2-Cu(II)-OH⁻ as the product state, rather than the widely-proposed state of the nitric oxide-bound T2-Cu(I)-NO⁺.^{7, 8, 16}

Conclusions

Using the combined MD simulations and the QM/MM-based metadynamics calculations (QM(B3LYP)/MM-MetD), we revisit the nitrite reduction mechanism in CuNiR by taking into account of the electron donor T1-Cu domain. The ET pathway analysis provides evidence that His135 and Cys136 are key residues involved in the intramolecular electron transfer from T1-Cu to T2-Cu. Upon the inclusion of electron donor T1-Cu domain, the reaction leads successfully to a PCET process, in which the proton transfer from Asp98 is coupled with the electron transfer from T1-Cu(I) to T2-Cu(II). Moreover, our calculations demonstrate that both Asp98 and His255 have to be protonated, in order to mediate a PCET process toward nitrite reduction.

QM(B3LYP)/MM-MetD provide interesting details about the nature of PCET reaction. It was found that ET process is driven by the conformation conversion of Asp98 from gatekeeper to proximal one, which is indeed much more energy-demanding than the PCET itself, while the latter process is quite facile starting from the proximal conformation of Asp98. Such conformational change triggered the ET from T1-Cu to T2-Cu, which in-turn drives the follow-up PT process. Finally, we show that product release occurs via a favorable HO---NO bond cleavage, leading to the T2-Cu(II)-OH⁻ as the product state, rather than the widely-proposed T2-Cu(I)-NO⁺ state.

Conflicts of interest

There are no conflicts to declare.

Acknowledgements

The grants from National Natural Science Foundation of China (No. 21933009, 21907082 and 21873078) to B. W and Z. C are acknowledged. The grant from the U.S. National Science Foundation (RUI-1904797) to C. W. is also acknowledged.

References

1. D. Fowler, M. Coyle, U. Skiba, M. A. Sutton, J. N. Cape, S. Reis, L. J. Sheppard, A. Jenkins, B. Grizzetti and J. N. Galloway, *Philos. T. R. Soc. B.*, 2013, **368**, 20130164.
2. N. Gruber and J. N. Galloway, *Nature*, 2008, **451**, 293-296.
3. D. E. Canfield, A. N. Glazer and P. G. Falkowski, *Science*, 2010, **330**, 192-196.
4. W. G. Zumft, *Microbiol. Mol. Biol. Rev.*, 1997, **61**, 533-616.
5. S. Horrell, D. Kekilli, R. W. Strange and M. A. Hough, *Metallomics*, 2017, **9**, 1470-1482.
6. E. I. Tocheva, F. I. Rosell, A. G. Mauk and M. E. Murphy, *Science*, 2004, **304**, 867-870.
7. E. I. Tocheva, F. I. Rosell, A. G. Mauk and M. E. Murphy, *Biochemistry*, 2007, **46**, 12366-12374.
8. S. V. Antonyuk, R. W. Strange, G. Sawers, R. R. Eady and S. S. Hasnain, *P. Natl. Acad. Sci. USA*, 2005, **102**, 12041-12046.
9. Y. Fukuda, K. M. Tse, T. Nakane, T. Nakatsu, M. Suzuki, M. Sugahara, S. Inoue, T. Masuda, F. Yumoto and N. Matsugaki, *P. Natl. Acad. Sci. USA*, 2016, **113**, 2928-2933.
10. T. P. Halsted, K. Yamashita, C. C. Gopalasingam, R. T. Shenoy, K. Hirata, H. Ago, G. Ueno, M. P. Blakeley, R. R. Eady and S. V. Antonyuk, *IUCrJ*, 2019, **6**, 761-772.
11. Y. Fukuda, Y. Hirano, K. Kusaka, T. Inoue and T. Tamada, *P. Natl. Acad. Sci. USA*, 2020, **117**, 4071-4077.
12. S. Brenner, D. J. Heyes, S. Hay, M. A. Hough, R. R. Eady, S. S. Hasnain and N. S. Scrutton, *J. Biol. Chem.*, 2009, **284**, 25973-25983.
13. N. G. Leferink, C. Han, S. V. Antonyuk, D. J. Heyes, S. E. Rigby, M. A. Hough, R. R. Eady, N. S. Scrutton and S. S. Hasnain, *Biochemistry*, 2011, **50**, 4121-4131.
14. N. G. Leferink, R. R. Eady, S. S. Hasnain and N. S. Scrutton, *FEBS J.*, 2012, **279**, 2174-2181.
15. M. Lintuluoto and J. M. Lintuluoto, *Biochemistry*, 2016, **55**, 4697-4707.
16. Y. Li, M. Hodak and J. Bernholc, *Biochemistry*, 2015, **54**, 1233-1242.
17. S. Ghosh, A. Dey, Y. Sun, C. P. Scholes and E. I. Solomon, *J. Am. Chem. Soc.*, 2009, **131**, 277-288.
18. M. Lintuluoto and J. M. Lintuluoto, *Biochemistry*, 2016, **55**, 210-223.
19. M. Lintuluoto and J. M. Lintuluoto, *Metallomics*, 2018, **10**, 565-578.
20. H. J. Wijma, L. J. Jeuken, M. P. Verbeet, F. A. Armstrong and G. W. Canters, *J. Biol. Chem.*, 2006, **281**, 16340-16346.
21. R. W. Strange, L. M. Murphy, F. E. Dodd, Z. H. Abraham, R. R. Eady, B. E. Smith and S. S. Hasnain, *J. Mol. Biol.*, 1999, **287**, 1001-1009.
22. M. E. Murphy, S. Turley and E. T. Adman, *J. Biol. Chem.*, 1997, **272**, 28455-28460.
23. M. J. Boulanger and M. E. Murphy, *Biochemistry*, 2001, **40**, 9132-9141.
24. K. Kobayashi, S. Tagawa and S. Suzuki, *J. Biochem. (Tokyo)*, 1999, **126**, 408-412.

25. Y. Zhao, D. A. Lukoyanov, Y. V. Toropov, K. Wu, J. P. Shapleigh and C. P. Scholes, *Biochemistry*, 2002, **41**, 7464-7474.
26. J. C. Cristaldi, M. C. Gómez, P. J. González, F. M. Ferroni, S. D. Dalosto, A. C. Rizzi, M. G. Rivas and C. D. Brondino, *BBA - Gen. Subjects*, 2018, **1862**, 752-760.
27. M. A. Hough, M. J. Ellis, S. Antonyuk, R. W. Strange, G. Sawers, R. R. Eady and S. S. Hasnain, *J. Mol. Biol.*, 2005, **350**, 300-309.
28. M. Kukimoto, M. Nishiyama, M. E. Murphy, S. Turley, E. T. Adman, S. Horinouchi and T. Beppu, *Biochemistry*, 1994, **33**, 5246-5252.
29. A. Laio and F. L. Gervasio, *Rep. Prog. Phys.*, 2008, **71**, 126601.
30. A. Barducci, G. Bussi and M. Parrinello, *Phys. Rev. Lett.*, 2008, **100**, 020603.
31. B. Ensing, A. Laio, M. Parrinello and M. L. Klein, *J. Phys. Chem. B*, 2005, **109**, 6676-6687.
32. H. J. Wijma, L. J. Jeuken, M. P. Verbeet, F. A. Armstrong and G. W. Canters, *J. Am. Chem. Soc.*, 2007, **129**, 8557-8565.
33. D. A. Case, T. E. Cheatham III, T. Darden, H. Gohlke, R. Luo, K. M. Merz Jr, A. Onufriev, C. Simmerling, B. Wang and R. J. Woods, *J. Comput. Chem.*, 2005, **26**, 1668-1688.
34. R. Dennington, T. A. Keith, and J. M. Millam, GaussView, Version 6.0.16, Semichem Inc., Shawnee Mission, KS, 2016.
35. M. J. Frisch, G. W. Trucks, H. B. Schlegel, G. E. Scuseria, M. A. Robb, J. R. Cheeseman, G. Scalmani, V. Barone, B. Mennucci, G. A. Petersson, H. Nakatsuji, M. Caricato, X. Li, H. P. Hratchian, A. F. Izmaylov, J. Bloino, G. Zheng, J. L. Sonnenberg, M. Hada, M. Ehara, K. Toyota, R. Fukuda, J. Hasegawa, M. Ishida, T. Nakajima, Y. Honda, O. Kitao, H. Nakai, T. Vreven, J. A. Montgomery, Jr., J. E. Peralta, F. Ogliaro, M. Bearpark, J. J. Heyd, E. Brothers, K. N. Kudin, V. N. Staroverov, R. Kobayashi, J. Normand, K. Raghavachari, A. Rendell, J. C. Burant, S. S. Iyengar, J. Tomasi, M. Cossi, N. Rega, J. M. Millam, M. Klene, J. E. Knox, J. B. Cross, V. Bakken, C. Adamo, J. Jaramillo, R. Gomperts, R. E. Stratmann, O. Yazyev, A. J. Austin, R. Cammi, C. Pomelli, J. W. Ochterski, R. L. Martin, K. Morokuma, V. G. Zakrzewski, G. A. Voth, P. Salvador, J. J. Dannenberg, S. Dapprich, A. D. Daniels, Ö. Farkas, J. B. Foresman, J. V. Ortiz, J. Cioslowski, and D. J. Fox, Gaussian 09, Gaussian, Inc., Wallingford CT, 2009.
36. P. Li and K. M. Merz Jr, *J. Chem. Inf. Model.*, 2016, **56**, 599-604.
37. J. A. Maier, C. Martinez, K. Kasavajhala, L. Wickstrom, K. E. Hauser and C. Simmerling, *J. Chem. Theory Comput.*, 2015, **11**, 3696-3713.
38. P. Mark and L. Nilsson, *J. Phys. Chem. A*, 2001, **105**, 9954-9960.
39. T.-S. Lee, D. S. Cerutti, D. Mermelstein, C. Lin, S. LeGrand, T. J. Giese, A. Roitberg, D. A. Case, R. C. Walker and D. M. York, *J. Chem. Inf. Model.*, 2018, **58**, 2043-2050.
40. R. Salomon-Ferrer, A. W. Götz, D. Poole, S. Le Grand and R. C. Walker, *J. Chem. Theory Comput.*, 2013, **9**, 3878-3888.
41. A. W. Götz, M. J. Williamson, D. Xu, D. Poole, S. Le Grand and R. C. Walker, *J. Chem. Theory Comput.*, 2012, **8**, 1542-1555.
42. S. Le Grand, A. W. Götz and R. C. Walker, *Comput. Phys. Commun.*, 2013, **184**, 374-380.
43. R. L. Davidchack, R. Handel and M. Tretyakov, *J. Chem. Phys.*, 2009, **130**, 234101.
44. H. J. Berendsen, J. v. Postma, W. F. van Gunsteren, A. DiNola and J. R. Haak, *J. Chem. Phys.*, 1984, **81**, 3684-3690.
45. U. Essmann, L. Perera, M. L. Berkowitz, T. Darden, H. Lee and L. G. Pedersen, *J. Chem. Phys.*, 1995, **103**, 8577-8593.
46. V. Kräutler, W. F. Van Gunsteren and P. H. Hünenberger, *J. Comput. Chem.*, 2001, **22**, 501-508.
47. J. Hutter, M. Iannuzzi, F. Schiffmann and J. VandeVondele, *Wires. Comput. Mol. Sci.*, 2014, **4**, 15-25.
48. J. VandeVondele, M. Krack, F. Mohamed, M. Parrinello, T. Chassaing and J. Hutter, *Comput. Phys. Commun.*, 2005, **167**, 103-128.
49. P. Wu, F. Fan, J. Song, W. Peng, J. Liu, C. Li, Z. Cao and B. Wang, *J. Am. Chem. Soc.*, 2019, **141**, 19776-19789.
50. A. Altun, J. Breidung, F. Neese and W. Thiel, *J. Chem. Theory Comput.*, 2014, **10**, 3807-3820.
51. M. R. Blomberg, T. Borowski, F. Himo, R.-Z. Liao and P. E. Siegbahn, *Chem. Rev.*, 2014, **114**, 3601-3658.
52. B. Wang, P. H. Walton and C. Rovira, *ACS Catal.*, 2019, **9**, 4958-4969.
53. S. Goedecker, M. Teter and J. Hutter, *Phys. Rev. B*, 1996, **54**, 1703.
54. M. Guidon, J. Hutter and J. VandeVondele, *J. Chem. Theory Comput.*, 2010, **6**, 2348-2364.
55. I. A. Balabin, X. Hu and D. N. Beratan, *J. Comput. Chem.*, 2012, **33**, 906-910.